Detection and Localization of Disconnections in PV Strings Using Spread Spectrum Time Domain Reflectometry

Mashad Uddin Saleh, *Student Member, IEEE*, Chris Deline, *Member, IEEE*, Samuel Kingston, *Student Member, IEEE,* Naveen Kumar Tumkur Jayakumar, *Student Member, IEEE,* Evan Benoit, *Student Member, IEEE,* Joel B. Harley, *Member, IEEE,* Cynthia Furse, *Fellow, IEEE*, Mike Scarpulla, *Senior Member, IEEE*

***Abstract*—This paper describes the novel use of spread spectrum time domain reflectometry (SSTDR) for detecting and locating disconnection faults in photovoltaic (PV) power plants. We measure strings of cells and full-sized modules to understand how disconnections affect the reflectometry signature. PV modules correspond to reactive loads and disconnections in a PV string and cause distinguishable and measurable changes in SSTDR responses. Disconnection faults are manually introduced and correctly identified and localized applying the proposed technique. The SSTDR technique can detect and locate disconnects through at least eight 36-cell modules. Using the new technique described in this paper, we can both detect and locate the disconnections within a 1-foot resolution, on average.**

***Index Terms*—PV string, PV cell, PV module, PV mini-module, solar cell, reflectometry, spread spectrum time domain reflectometry, SSTDR, fault location, disconnection.**

I. INTRODUCTION

ELECTRICAL disconnections in photovoltaic (PV) arrays are common problems in industrial and residential PV power plants [1]. These may be caused by damage to the cables or connectors, corrosion in the connectors, poor mechanical connections leading to poor electrical connections, and related problems. Disconnections can also occur due to short circuits or ground faults. PV arrays are typically connected to the grid through inverters, and disconnections cause problems when they disrupt the total power flow to the grid [2] or to an individual device. Detecting and locating these faults is crucial to maintaining a consistent flow of power.

Various techniques are used to detect faults and disconnections in PV strings. Current and voltage (IV) monitoring can alert operators to problems at the string level, but cannot readily localize these disconnections [3]. Electroluminescence [4], [5], visual inspection [4] and infrared (IR) imaging even from platforms like unmanned aerial vehicle [6] are useful for finding damage in the modules themselves, however, are unable to see issues with cabling behind the modules [7]. In this paper, we will evaluate the ability of electrical reflectometry, specifically spread spectrum time domain reflectometry (SSTDR), to both detect and locate disconnections in PV systems. Unlike IV testing, which monitors the net current and/or voltage on the system, time of flight reflectometry techniques like SSTDR monitor the spatial arrangements of impedances and any changes thereof. This spatial monitoring is key to locating faults.

Time-domain reflectometry (TDR) techniques are commonly used to detect and locate faults, including disconnections, in electrical systems [8]. Previously, TDR has been used to detect faults in PV systems [9], however, the detection and location accuracy was limited in part by the electrical noise in the system, and the technique cannot be applied in live PV systems. TDR often uses transforms to locate faults, and these can also be applied to SSTDR to improve the accuracy of fault location [10]. In reflectometry, an electromagnetic signal is sent through the system, and reflections from impedance discontinuities return to the test end, where they are analyzed to produce a reflectometry signature. The time delays between the incident signal and the various reflections indicate the distances to the discontinuities, and magnitude and phase of the reflected signal are related to the type of impedance discontinuity. Each type of reflectometry uses a different type of incident signal and method of analyzing the reflections. SSTDR uses modulated pseudo-noise (PN) codes and time correlation techniques. It can be applied to live (energized) systems without disturbing normal system operation, as the test signal can be within the noise margin of the operating DC or AC voltages [11]. Changes such as irradiance and bypass diodes are detectable but produce reflections that are smaller than the disconnections that will be seen in this paper. These factors were held constant in the experiments while only the connection was changed.

SSTDR has been previously used to detect ground faults [12] and arc faults [13] in PV systems, using averaging algorithms for detection but not the location of these faults. In this paper, we will focus on the reflectometry signatures themselves, and how they may be used for diagnosing and locating disconnections in PV systems. For frequency-independent faults such as open and short circuits and resistive loads, this method is straightforward, however for frequency-dependent impedances such as capacitors or inductors, this is much more complicated. For complex impedances, not only does the magnitude of the time domain signature depend on the impedance, but also the shape of the signature changes. PV cells can be modeled as a combination of series resistance, series inductance, shunt resistance and shunt capacitances [14], [15]. At lower frequencies (<1 MHz approximately), the PV cells act like capacitive elements, and at higher frequencies (especially at the10-50 MHz frequencies used for SSTDR in this paper)

they are dominated by inductances. As a result, SSTDR signatures for PV systems fall into this more complicated category. We will evaluate disconnections within these systems. Other types of damage, such as damage to the cells or modules themselves, will be the topic of future work.

This paper evaluates the measured SSTDR signature of PV systems, starting from the cell level and extending to the module level. Custom mini-modules consisting of one and two cells were fabricated and tested, as described in section II. SSTDR responses for larger PV modules are described in section III. Then, breaks in strings of PV modules are measured, and a method to detect and localize breaks at the string level is demonstrated in section IV.

II. SSTDR Responses From PV Cells

Spread spectrum time domain reflectometry (SSTDR) [16] sends a square-wave modulated pseudo-noise (PN) code down a cable, where it reflects off impedance discontinuities. The reflected signal returns to the SSTDR instrument, where it is cross-correlated with a delayed version of the incident signal to create the reflectometry response. In this paper, we will show the reflectometry responses for various loads (open, short, capacitor, inductor, PV cells, modules) connected to PV cable configured as a twin lead cable, as shown in Fig. 1(a). In this section, we will evaluate and compare the reflection signatures from these loads to demonstrate how they can be used to diagnose the loads and disconnection faults.

Table I
PV cable [17] and SSTDR parameters

Parameters	Values
Conductor diameter (d_c)	2.94 mm
Conductivity of copper(σ_c)	5.98×10^7 S/m
Loss tangent of XLPE	4×10^{-4}
$\mu_{r_{XLPE}}$	0.999994
XLPE insulation thickness (t_{in})	3.375 mm
Distance between conductors (D_c)	11 mm
$\varepsilon_{r_{XLPE}}$	2.3
Z_{SSTDR}	68 Ω
f_m	24 MHz
v_o	0.722 ± 0.008
Z_o	178 Ω
Z_{SSTDR}	68 Ω

The twin lead cable was made up of 10 AWG multi-conductor cross-linked polyethylene (XLPE) coated 2000 V PV wires [17] taped together to form a twin-lead cable. The method described in this paper is relatively independent of wire type. This is because we take a baseline reflectometry signature on an initial good (fault-free) system and later subtract it from the reflectometry signature from a faulted system. This removes the reflections caused the junction between the reflectometer and wire, connectors, and any other impedance mismatches in the system. Then the reflection from only the fault can be analyzed. The parameters of this twin-lead cable are given in Table I. To find its characteristic impedance, we attached a potentiometer as the load and tuned it until reflections were not visible. This gave Z_o = 178 Ω. The velocity of propagation, v_o = 0.722 ± 0.008 times the speed of light (c_o), was found by measuring the SSTDR response of an open circuit on a known length of cable [18]. Over the frequency range from 12kHz to 48MHz the velocity of propagation would be expected to vary less than 0.13% on the transmission lines. Data is not available for expected frequency dispersion within the modules, however, given that neither the material properties nor the spatial configuration varies significantly with frequency we can expect the velocity of propagation through the modules to be relatively insensitive to frequency.

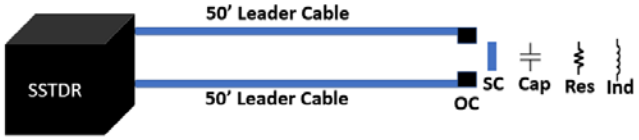

(a)

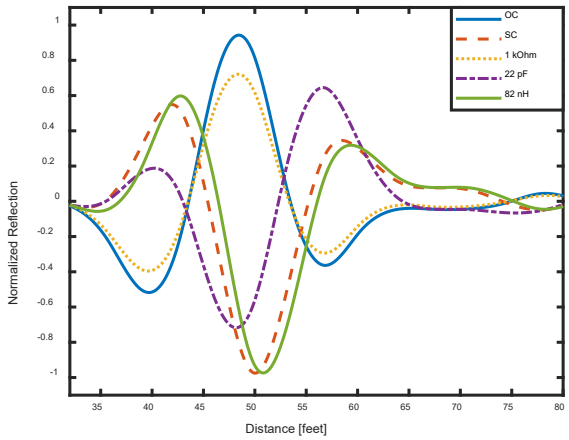

(b)

Fig 1. Measured SSTDR reflection responses for a simple test system (a). The smoothed and normalized SSTDR responses (b) are shown for various loads.

For our tests, we used an ARNOLD W50A0093 SSTDR instrument from LiveWire Innovation Inc. [19]. Its characteristic impedance is Z_{SSTDR} = 68 Ω. The SSTDR is run in 24 MHz continuous mode, which uses a 24 MHz PN code modulated by a 24 MHz square wave. 24 MHz was chosen because it provides sufficient resolution over the total length of the PV system. The SSTDR signature is shown in Fig. 1(b) for an open circuit load 50 ft from the SSTDR. Higher frequency would produce a narrower spatial reflection signature for better resolution but would attenuate more quickly and therefore have a more limited distance over which faults can be detected. The SSTDR signature is normalized to the magnitude of the open circuit response at this location, which removes effects of attenuation on the cable. A similar negative signature is seen for a short circuit load. The distance (from the SSTDR) was calculated by taking the measured time delay and dividing by the velocity of propagation, v_o. We smoothed and spline interpolated the peaks as described in [18] for improved accuracy. In addition to the reflection signatures shown at the load, there is always a similar pulse at the impedance

discontinuity from the SSTDR instrument to the transmission line (distance =0), which we have not shown.

The SSTDR signatures using the experimental setup from Fig. 1(a) for open circuit (OC), short circuit (SC) and a resistive load (1 kΩ) change the magnitude, but not the shape of the SSTDR reflection signature. However, capacitive (22 pF) and inductive loads (82 nH) change the shape of the signature, showing representative reflectometry signatures. Depending on the frequency range, as the capacitance increases, the bottom lobe decreases and moves to the right, and the overall signature transitions from a near-open circuit (for small capacitors) to become more and more like a short circuit (for large capacitors). This is consistent with the impedance of a capacitor $Z_c = 1/j\omega C$. A similar reverse effect can be seen for an inductor with load impedance ($Z_L = j\omega L$).

A. Single Cell PV Mini-modules

In this section, we will show the SSTDR response for series combinations of single-cell PV mini-modules. The cell parameters are given in Table II. To completely understand the reflectometry behavior inside a full-sized module, we have to first understand the behavior of a single unit, such as a single cell mini-module.

Table II
Single cell mini-module parameters

Parameters	Values
Cell area	244.2 cm^2 ± 0.1%
V_{OC}	0.6267 ± 0.0011 V
I_{SC}	9.035 ± 0.055 A
I_{max}	8.542 ± 0.052 A
V_{max}	0.527854 ± 0.000074 V
P_{max}	4.509 ± 0.028 W

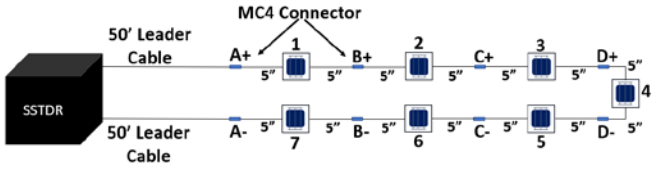

(a)

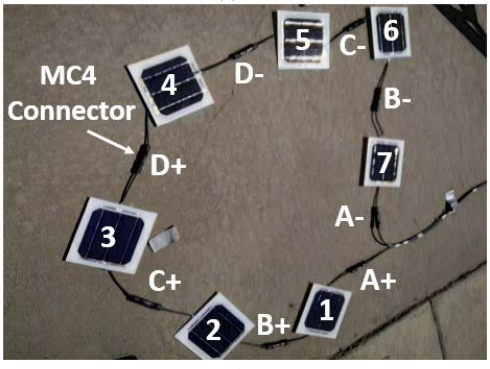

(b)

Fig 2. (a) Schematic for the setup of seven single-cell PV mini-modules connected in series, (b) Photograph of how the string of cells is laid out.

We created mini-modules with either one or two cells encapsulated in the same way as typical PV modules are made [20]. The PV cell is covered by glass, followed by an ethylene vinyl acetate (EVA) layer. The cells (6-inch by 6-inch polycrystalline silicon solar cells similar to [21]) were soldered to bussbars covered by EVA and then covered with a Tedlar backsheet. MC4 connectors were soldered to the lead tabs.

Seven single-cell PV mini-modules were fabricated and connected in the ring configuration shown in Fig. 2. An MC4 connector joined each mini-module at points B+, C+, etc. Fig. 3 shows the SSTDR responses as mini-modules were sequentially added to the ring under direct outdoor illumination. Connecting multiple mini-modules in series increases the total impedance as we can see in Fig. 3, where the lower lobe increases as single-cell mini-modules are added. This reflection signature moves to the right, consistent with additional delays from each additional length of wire and mini-module. There is also a notable change in the shape in the signature caused by frequency dispersion from the frequency dependent impedance of the mini-modules.

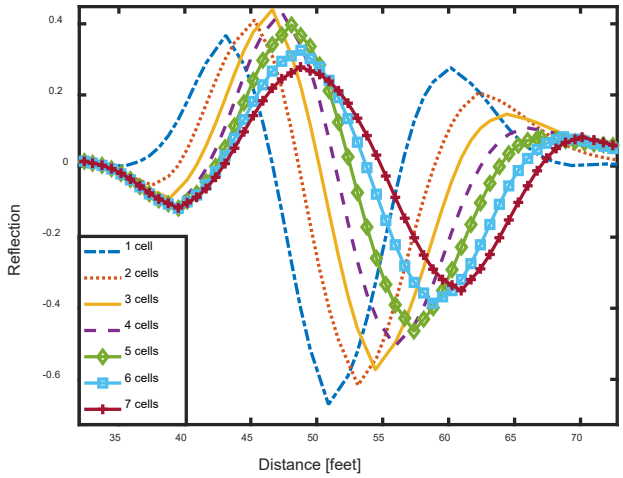

Fig 3. SSTDR responses for series connections of single-cell mini-modules (up to 7) in the configuration shown in Fig. 2. Measurements were taken outside in full sun.

These tests show that increasing the number of PV cells in series increases the impedance of the system, which in turn shows up in the SSTDR responses. This can be used to determine where the system is disconnected by comparing initial tests (a baseline when all the cells are properly connected) to a later test (when a break appears in the line, disconnecting some of the cells), as will be described in the following section.

III. SSTDR Reponses From PV Modules

The mini-module tests in the previous section give us a general idea of what to expect in the SSTDR responses of full PV modules. A module is a series connection of many cells, and more modules mean more cells, which translates to more impedance in series, and small delays between cells.

This effect can be seen by testing full-sized PV modules. PV modules with 36 cells from Renogy (RNG100D) [22] were connected as shown in Fig. 4(a). The modules consist of 4 columns of 9 cells organized into 2 strings with one bypass diode. The associated SSTDR responses are shown in Fig. 4(b),

and the differences as each module is added are shown in Fig. 4(c). Like the mini-modules, we see a change in the SSTDR signature as each module is added.

Comparing the baseline response when all modules are connected to a response when a module is disconnected (Fig. 4(c)) shows a difference that would allow the detection of that removal. One way of localizing breaks in the system would be to collect SSTDR signatures as each module is added (such as during installation) and then compare those with data collected after a fault is detected (using a lookup table), but we will describe an alternative approach below.

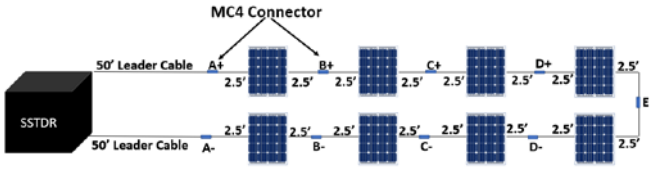

(a)

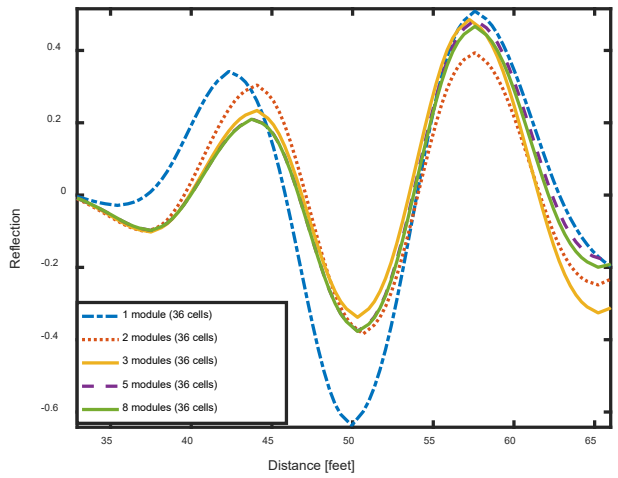

(b)

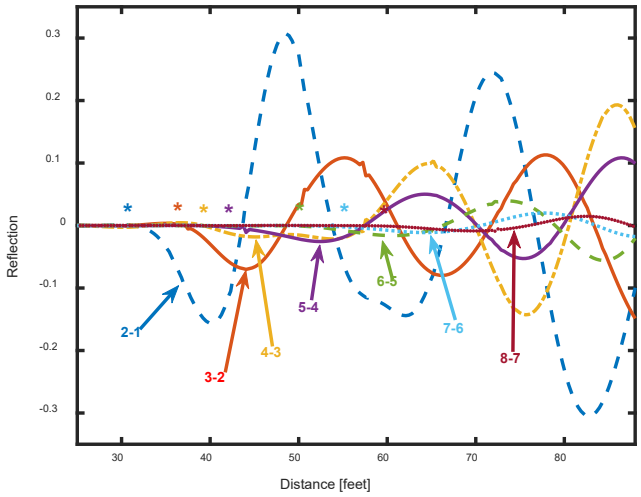

(c)

Fig 4. (a) Schematic of eight 36-cell PV modules connected in series, (b) SSTDR responses as each module is added, (c) Difference of the SSTDR signatures as each module is added (e.g. 2-1 denotes the response for 2 modules minus the response for 1 module, etc.).

There are two important conclusions from these tests, which can be seen primarily in the difference plots (Fig. 4(c)). First, changes are seen when each module is added, indicating that the SSTDR signal effectively passed through all the modules, returning to the test point. This is essential for being able to test for faults in the system. We also tested 60-cell modules from Peimar SG300M [23] (results not shown), and although the responses were smaller than for the 36-cell modules, we were able to detect disconnections through at least nine of these 60-cell modules. Comparing these module results to the mini-module (single cell) results in Fig. 3, we see similar shapes of the reflection signature, however, the location at which the signature leaves the baseline is longer for the modules than the cells. This is because the modules are themselves longer and have more delay than the individual cells.

Another important observation is that the point at which the difference signal deviates from zero moves further away from the instrument as each module is added. For instance, by comparing the data for (2-1) and (3-2) and using the v_o of the cable to calculate the distance in feet, the equivalent length for each module and its associated connecting cables is approximately 6.5 feet for these modules. This equivalent length is very different from the path length of the DC current path through the module (estimated at >20 ft) because of the complex electric field distribution as the signal passes through the module and for now must be empirically determined. Later differences are also delayed, however the multiple reflections within the system make the signatures and hence differences more complex, so the delay is harder to analyze. More advanced analysis algorithms are needed for larger systems and will be the subject of future work.

IV. Disconnections In the System

In the previous sections, we evaluated how adding cells or modules impacts the SSTDR signatures by adding length and multiple reflections. In this section, we will examine the effect of disconnections between the modules. This is slightly different from the previous section, and from traditional reflectometry literature because the remaining modules are still present. For instance, if a break is made at B+, the connection at B- is still there. This creates an asymmetric transmission line system [24]. The SSTDR hardware we are using is also asymmetric, as a circuit protection filter exists on the positive (but not the negative) terminal to enable testing on live (energized) DC systems. This frequency-dependent filter slightly changes the shape and delay of the SSTDR signatures on the positive terminal but not on the negative terminal, as we will see in the following disconnection tests. This has the advantage of allowing us to distinguish between otherwise identical disconnections on the positive and negative lines, however, this must be accounted for in the data analysis.

A. Detecting Disconnections in Series Connected PV Single-cell Mini-modules

The setup in Fig. 2(a) shows seven individual PV cells connected in a ring configuration. The MC-4 connectors on the positive line are A+, B+, C+, and D+, and the connectors on the negative line are A-, B-, C- and D-. SSTDR responses for disconnections at each of these locations are shown in Fig. 5

(a). Breaks at A+/A- are clearly seen as open circuits (See Fig. 1 for the shape of an open circuit response). Other break locations create overlapping reflections. Slight differences are seen between A+ and A-, B+ and B-, etc., as expected from this asymmetric system. In traditional reflectometry analysis, the location of the disconnection would be identified by the location of the peak, as for the A+/A- breaks. However, for later breaks overlapping reflections change the waveform shape and preclude that type of analysis. Instead, we can determine the relative location of the breaks by comparing the "No break" baseline and the disconnection signature, and identifying where they diverge as shown in Fig. 5(b). We will apply this concept to locating breaks between full PV modules in the next section.

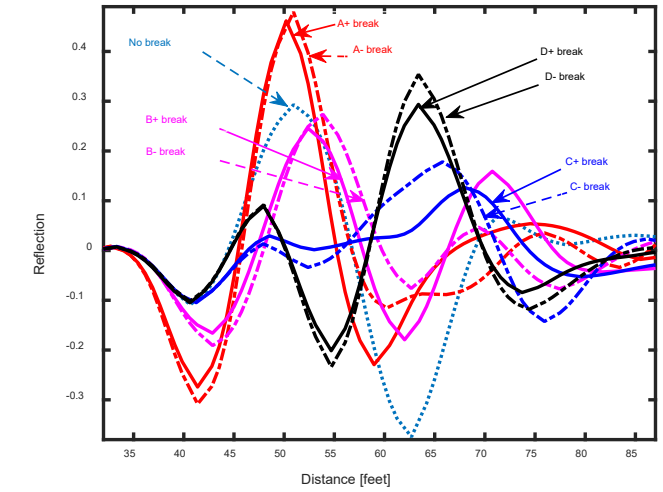

(a)

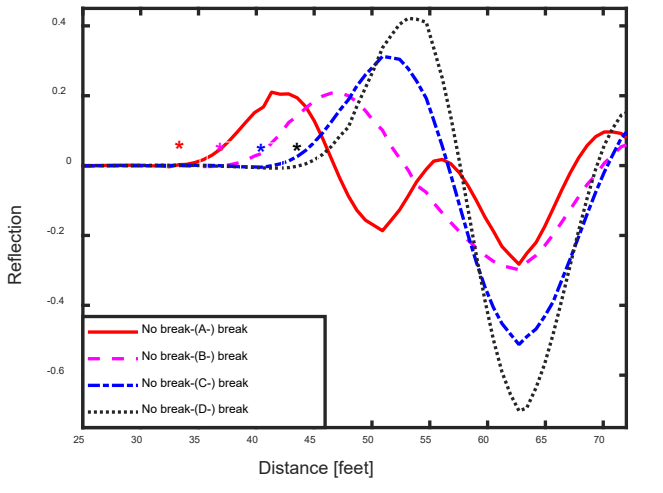

(b)

Fig 5. (a) SSTDR responses for disconnections at each break in the series connection of seven individual cells shown in Fig. 2. (b) Differences of SSTDR responses relative to no break condition. Measurements were taken outside in full sun.

B. Detecting Disconnections in Series Connected PV Modules

Reflectometry responses for eight 36-cell Renogy PV modules connected in series as in Fig. 4(a) are shown in Fig. 6(a). We can then subtract signatures with breaks (MC-4 connectors disconnected at specific locations) from the "No break" baseline signature, as shown in Fig. 6(b). Similar to the previous results from individual single-cell mini-modules, the A+ and A- disconnections look like open circuits, with asymmetry between the positive and negative lines. The relative locations of later disconnections can be found from the locations where the "No break" baseline and the reflection signatures diverge. Changes are observed for differences from baseline (Fig. 6(b)) for all breaks up to eight modules. Using the baseline subtraction method (Fig. 6(b), breaks can be seen at all locations for eight 36-cell Renogy modules, although baseline subtraction responses are smaller for breaks further from the SSTDR instrument because of attenuation and multiple reflections. We also made similar tests (not shown) for modules from Siemens. We saw the same effects (variation with shape and the divergence from the baseline proportional to the distance to the disconnection), although the specific reflection signatures were significantly different in their details due to different number and configuration of bussbars, the size, and doping of the cells, etc. Next, we will describe an algorithm for determining the locations of these breaks. This is extremely helpful information that cannot be easily determined on series-connected modules from simple monitoring techniques such as examining power output.

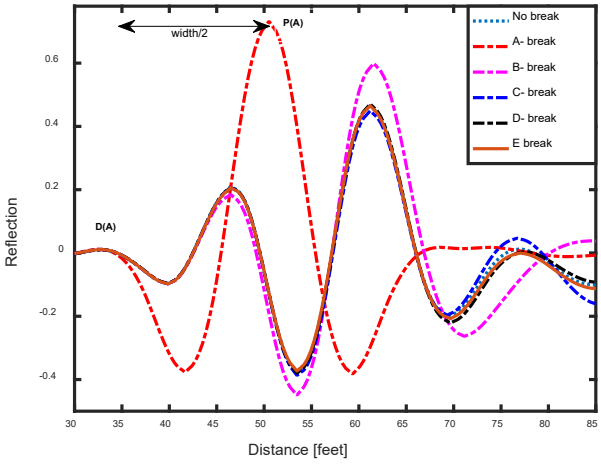

(a)

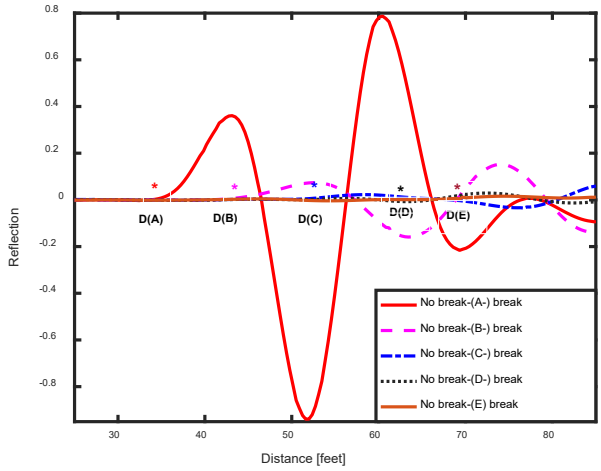

(b)

Fig 6. (a) SSTDR responses for disconnections at each break in the series connection of eight 36-cell Renogy PV modules (b) Differences of SSTDR

responses relative to no break condition. Schematic of the setup is shown in Fig. 4 (a).

Similar to Fig. 5(b), we can use the "No break" signature in Fig. 6(a) as a baseline and subtract each disconnection signature from it, to give the subtracted signatures in Fig. 6(b). We can then identify the locations where the SSTDR signatures diverge from the baseline, shown as D(A), D(B), etc. These divergence locations are associated break location (i.e. A-, B-, etc.); we have not yet found the magnitudes to be as effective for determining break location. This divergence location (given in Table III) is related to the location of the break. Adding half of the width of the SSTDR pulse signature (the distance between *P(A)* and *D(A)* shown in Fig. 6(a)) will give the apparent location of the disconnection in feet (also given in Table III):

$$L(x) = D(x) + \big(P(A) - D(A)\big) \; for \; x = B-, C-, etc. \quad (1)$$

Table III Localization of disconnection
Breaks: x, Divergence Location (feet): D(x), Apparent Disconnection Location (feet): L(x), Effective Length/Cell Length (feet): L_{eff}

(seven Single-cell mini-modules connected in series, see Fig. 2 (a))

x	*D(x) (From Fig. 5(b))*	*L(x)*	L_{eff}	Actual Disconnection Location	Location Accuracy (in feet)
A-	34.7	50.5	-	50.5	0 feet
B-	38.3	54.2	3.7 / 2.9	54.2	0 feet
C-	42.1	57.9	3.7 / 2.9	57.9	0 feet
D-	44.3	60.1	2.2 * / 1.4	61.6	1.5 feet

* Due to the odd number of single-cell mini-modules, this includes half as much distance through modules.

(eight Renogy modules connected in series, see Fig. 4 (a))

x	*D(x) (From Fig. 6(b))*	*L(x)*	L_{eff}	Actual Disconnection Location	Location Accuracy (in feet)
A-	35.0	50.5	-	50.5	0 feet
B-	43.9	59.4	8.9 /3.9	59.4	0 feet
C-	53.5	69.0	9.6 / 4.6	68.3	0.7 feet
D-	63.4	78.9	9.9 / 4.9	77.2	1.7 feet
E	69.3	84.8	5.9 / -	86.1	1.3 feet

For our algorithm, we identified the divergence locations using two different methods. First, when the magnitude of the subtracted waveforms exceeds 1% magnitude change of the SSTDR response from the open circuit condition. As an example, in Fig. 6 (a), the D (A) indicates where the (No break – (A-) break) has 1% magnitude change and so on for D(B), D(C), etc. The results of this algorithm are tabulated in Table III. While the subtracted data have very low magnitude, we need a more robust algorithm to identify the divergence point as a fixed threshold will not be appropriate for all the datasets. Another way to detect the beginning of divergence is to apply a moving threshold in a specified moving window through the whole data set [25], however this did not improve our accuracy. Future work on improved divergence detection algorithm is recommended.

The total effective length (L_{eff}) traversed by the SSTDR signal across one PV module and its associated connection cables can be approximated by:

$$L_{eff} = D(x+1) - D(x) \qquad x = A-, B-, C- etc. \quad (2)$$

The effective length is different from the physical length because all of the calculations above use distances calculated using the velocity of propagation of the cable. The velocity of propagation of the transmission line formed between a module and a return cable or a module and another module on the DC return path is unknown. We use the velocity of propagation from the cable throughout the entire system, thus providing only a relative length through the module, rather than an absolute physical length. The results for series connections of seven single-cell mini-modules and eight (36-cell) Renogy modules are shown in Table III.

V. Conclusions

We evaluated the reflectometry responses from series-connected PV single-cell mini-modules and strings of module to identify and locate disconnection faults within these systems. SSTDR reflectometry signatures confirm that PV cells are inductive at higher frequencies (approximately more than 1 MHz). When cells are connected in series, the impedance increases as PV cells are added. In addition, wires connecting them add slight delays. Similar effects are seen when adding series-connected PV modules. However, as we add more cells (more modules), the reflectometry signal is attenuated, and multiple reflections overlap, making the signature more difficult to analyze for increasing numbers of modules. To improve this analysis, we used a baseline subtraction method where signatures from faulty systems are subtracted from signatures for fault-free systems, and this difference is analyzed.

This allowed us to see through and identify disconnection locations for at least eight 36-cell modules and at least nine 60-cell modules. We were able to locate the disconnection position within 1-foot accuracy on an average. PV systems are often made up of combinations of parallel strings of series connected modules. Parallel systems should be expected to behave as a branched network [11]. Signals from each arm of the branch split and create an overlapping signature where this or similar algorithm will be even more important.

For actual implementation, several additional issues need to be addressed. The SSTDR method proposed can be embedded in each inverter or string converter, is capable of running on live, energized systems, and is therefore proposed for detecting long-standing (hard) disconnections as well as intermittent disconnections. This method has been shown to be immune to changes in voltage or current from load changes [26], however switching the load in or out causes impedance changes that

would be detectable. The system would need information on the timing of switching changes, so that they could be ignored. This method is expected to be installed (embedded) in PV systems. SSTDR circuitry could be embedded at the time of installation of the PV system. This would allow the most accurate baseline to be taken, stored, and used.

Additional analysis is needed to understand how the physical configuration of the system (series vs. parallel PV strings, configurations of bypass diodes, poor soldering etc.) may affect the results.

ACKNOWLEDGMENT

This material is based upon work supported by the U.S. Department of Energy's Office of Energy Efficiency and Renewable Energy (EERE) under Solar Energy Technologies Office (SETO) Agreement Number DE-EE0008169. Also, we want to express our gratitude to Gardner Energy (West Haven, UT) for their support in conducting testing on their PV modules.

DISCLOSURE

Dr. C.M. Furse is a co-founder of LiveWire Innovation, Inc. which is commercializing SSTDR technology, and therefore has a financial conflict of interest with this company.

REFERENCES

[1] M. A. Eltawil and Z. Zhao, "Grid-connected photovoltaic power systems: Technical and potential problems—A review," *Renew. Sustain. Energy Rev.*, vol. 14, no. 1, pp. 112–129, 2010.

[2] M. E. Ropp, M. Begovic, and A. Rohatgi, "Prevention of islanding in grid-connected photovoltaic systems," *Prog. Photovolt. Res. Appl.*, vol. 7, no. 1, pp. 39–59, 1999.

[3] E. Roman, R. Alonso, P. Ibañez, S. Elorduizapatarietxe, and D. Goitia, "Intelligent PV module for grid-connected PV systems," *IEEE Trans. Ind. Electron.*, vol. 53, no. 4, pp. 1066–1073, 2006.

[4] J. A. Tsanakas, L. Ha, and C. Buerhop, "Faults and infrared thermographic diagnosis in operating c-Si photovoltaic modules: A review of research and future challenges," *Renew. Sustain. Energy Rev.*, vol. 62, pp. 695–709, 2016.

[5] A. Mellit, G. M. Tina, and S. A. Kalogirou, "Fault detection and diagnosis methods for photovoltaic systems: A review," *Renew. Sustain. Energy Rev.*, vol. 91, pp. 1–17, 2018.

[6] P. B. Quater, F. Grimaccia, S. Leva, M. Mussetta, and M. Aghaei, "Light Unmanned Aerial Vehicles (UAVs) for Cooperative Inspection of PV Plants," *IEEE J. Photovolt.*, vol. 4, no. 4, pp. 1107–1113, Jul. 2014.

[7] A. Triki-Lahiani, A. B.-B. Abdelghani, and I. Slama-Belkhodja, "Fault detection and monitoring systems for photovoltaic installations: A review," *Renew. Sustain. Energy Rev.*, vol. 82, pp. 2680–2692, 2018.

[8] C. Furse, Y. C. Chung, C. Lo, and P. Pendayala, "A critical comparison of reflectometry methods for location of wiring faults," *Smart Struct. Syst.*, vol. 2, no. 1, pp. 25–46, 2006.

[9] T. Takashima, J. Yamaguchi, K. Otani, T. Oozeki, K. Kato, and M. Ishida, "Experimental studies of fault location in PV module strings," *Sol. Energy Mater. Sol. Cells*, vol. 93, no. 6–7, pp. 1079–1082, 2009.

[10] J. Zhang, Y. Zhang, and Y. Guan, "Analysis of time-domain reflectometry combined with wavelet transform for fault detection in aircraft shielded cables," *IEEE Sens. J.*, vol. 16, no. 11, pp. 4579–4586, 2016.

[11] C. Furse, P. Smith, C. Lo, Y. C. Chung, P. Pendayala, and K. Nagoti, "Spread spectrum sensors for critical fault location on live wire networks," *Struct. Control Health Monit. Off. J. Int. Assoc. Struct. Control Monit. Eur. Assoc. Control Struct.*, vol. 12, no. 3–4, pp. 257–267, 2005.

[12] M. K. Alam, F. Khan, J. Johnson, and J. Flicker, "PV ground-fault detection using spread spectrum time domain reflectometry (SSTDR)," in *2013 IEEE Energy Conversion Congress and Exposition*, Denver, CO, USA, 2013, pp. 1015–1020.

[13] M. K. Alam, F. H. Khan, J. Johnson, and J. Flicker, "PV arc-fault detection using spread spectrum time domain reflectometry (SSTDR)," in *2014 IEEE energy conversion congress and exposition (ECCE)*, 2014, pp. 3294–3300.

[14] D. Chenvidhya, K. Kirtikara, and C. Jivacate, "PV module dynamic impedance and its voltage and frequency dependencies," *Sol. Energy Mater. Sol. Cells*, vol. 86, no. 2, pp. 243–251, 2005.

[15] M. U. Saleh *et al.*, "Signal Propagation Through Piecewise Transmission Lines for Interpretation of Reflectometry in Photovoltaic Systems," *IEEE J. Photovolt.*, vol. 9, no. 2, pp. 506–512, 2019.

[16] P. Smith, C. Furse, and J. Gunther, "Analysis of spread spectrum time domain reflectometry for wire fault location," *IEEE Sens. J.*, vol. 5, no. 6, pp. 1469–1478, 2005.

[17] "'Spec 5851 SunGen XLPE, Photovoltaic Wire, 2000 V, UL Type PV or 1000 V, CSA RPVU90, Single Conductor, Copper.' [Online]. Available: http://dtsheet.com/doc/1724396/spec-5851-sungen-xlpe--photovoltaic-wire--2000-v--ul-type... [Accessed: 23-Aug-2018]." .

[18] N. K. T. Jayakumar *et al.*, "Post-Processing for Improved Accuracy and Resolution of Spread Spectrum Time Domain Reflectometry (SSTDR)," *IEEE Sens. Lett.*, 2019.

[19] "'Live Cable Fault Detection by LiveWire Innovation,' LiveWire Innovation. [Online]. Available: http://www.livewireinnovation.com/. [Accessed: 07-May-2018]." .

[20] J. Pern, "Module encapsulation materials, processing and testing (presentation)," National Renewable Energy Lab.(NREL), Golden, CO (United States), 2008.

[21] "Aliexpress.com | Alibaba Group," *aliexpress.com*. [Online]. Available: https://www.aliexpress.com/item/Energia-Solar-Direct-2016-Promotion-10pcs-High-Efficiency-4-33w-Poly-Solar-Cell-6x6-for-Diy/32626393408.html?src=ibdm_d03p0558e02r02&sk=&aff_platform=&aff_trace_key=&af=&cv=&cn=&dp=. [Accessed: 30-Dec-2018].

[22] "Renogy 100 Watt 12 Volt Monocrystalline Solar Panel," *Renogy*. [Online]. Available: https://www.renogy.com/renogy-100-watt-12-volt-monocrystalline-solar-panel/. [Accessed: 29-Dec-2018].

[23] "Peimar Group SG300M | Reviews and Ratings | EnergySage." [Online]. Available: https://www.energysage.com/panels/Peimar+Group/SG300M/. [Accessed: 02-Apr-2019].

[24] M. U. Saleh *et al.*, "Reflectometry on Asymmetric Transmission Line Systems (submitted to Progress in Electromagnetics Research)."

[25] J. B. Harley and J. M. Moura, "Data-driven and calibration-free Lamb wave source localization with sparse sensor arrays," *IEEE Trans. Ultrason. Ferroelectr. Freq. Control*, vol. 62, no. 8, pp. 1516–1529, 2015.

[26] C. Furse, P. Smith, M. Safavi, and C. Lo, "Feasibility of spread spectrum sensors for location of arcs on live wires," *IEEE Sens. J.*, vol. 5, no. 6, pp. 1445–1450, 2005.